

Dark matter halo abundances, clustering and assembly histories at high redshift

J.D. Cohn¹ and Martin White²

¹*Space Sciences Laboratory,*

²*Departments of Physics and Astronomy,
University of California, Berkeley, CA 94720*

1 November 2018

ABSTRACT

We use a suite of high-resolution N-body simulations to study the properties, abundance and clustering of high mass halos at high redshift, including their mass assembly histories and mergers. We find that the analytic form which best fits the abundance of halos depends sensitively on the assumed definition of halo mass, with common definitions of halo mass differing by a factor of two for these low concentration, massive halos. A significant number of massive halos are undergoing rapid mass accretion, with major merger activity being common. We compare the mergers and mass accretion histories to the extended Press-Schechter formalism.

We consider how major merger induced star formation or black hole accretion may change the distribution of photon production from collapsed halos, and hence reionization, using some simplified examples. In all of these, the photon distribution for a halo of a given mass acquires a large scatter. If rare, high mass halos contribute significantly to the photon production rates, the scatter in photon production rate can translate into additional scatter in the sizes of ionized bubbles.

1 INTRODUCTION

Observations of the anisotropy of the cosmic microwave background (CMB) radiation have given us unprecedented knowledge of the very early Universe and dramatically confirmed the picture of large-scale structure as arising from the gravitational amplification of small perturbations in a Universe with a significant cold dark matter component (Smoot et al. 1992). In this model the ionization history of the Universe has two main events, a ‘recombination’ at $z \sim 10^3$ in which it went from ionized to neutral and a ‘reionization’ during $z \sim 7 - 12$ in which the radiation from early generations of collapsed objects was able to ionize the intergalactic medium. The former event is strongly constrained by the CMB. A new generation of instruments will soon allow us to probe this second event: “the end of the dark ages” (for reviews of reionization see e.g. Barkana & Loeb 2001; Cooray & Barton 2006; Fan, Carilli & Keating 2006; Furlanetto, Oh & Briggs 2006).

Since at reionization a very small fraction of the mass affected each and every baryon in the Universe, reionization is particularly sensitive to the distribution and behavior of collapsed structure. We expect that the ionizing sources are situated in large ($T_{\text{vir}} > 10^4\text{K}$ or $M > 10^7 h^{-1} M_{\odot}$) dark matter halos where the gas can cool efficiently to form stars¹. Models for the sources of reionization thus often start with

estimates of the number and properties of virialized dark matter halos at high redshift, the focus of this paper. At $z = 10$, halos with $M > 10^9 h^{-1} M_{\odot}$ are expected to be biased similarly to very massive clusters ($M > 10^{15} h^{-1} M_{\odot}$) today, with the most massive and recently formed halos growing rapidly and merging frequently. We explore some properties of these collapsed halos at a high redshift using a suite of high resolution, collisionless, N-body simulations. We pay particular attention to merger rates and mass accretion histories with an eye to applications for reionization. We also compare the N-body results with the predictions of the oft-used Press & Schechter (1974) formalism.

If halo mergers are accompanied by a temporary increase in photon production (due either to starbursts or increased black hole accretion e.g. Carlberg 1990; Barnes & Hernquist 1991, 1996; Mihos & Hernquist 1994, 1996; Kauffmann & Haehnelt 2000; Cavaliere & Vittorini 2000) we expect reionization to be influenced by the merger and accretion history of dark matter halos, beyond just the fact that more massive halos emit more photons. With a simple model of star formation we show that merger-induced scatter in photon production may be significant, with the production rates acquiring a substantial tail to large photon production rates. Since the massive halos are relatively rare, this individual halo scatter is expected to translate into a scatter of photon production rates inside ionized regions, changing the bubble distribution.

The outline of the paper is as follows. In §2 we describe the N-body simulations. The basic halo properties are described in §3 along with the results for mergers and mass

¹ We will only consider Pop II stars here; Pop III stars, which can form in the absence of metals in smaller halos, are expected to be less likely by redshift 10 (Yoshida, Bromm & Hernquist 2004).

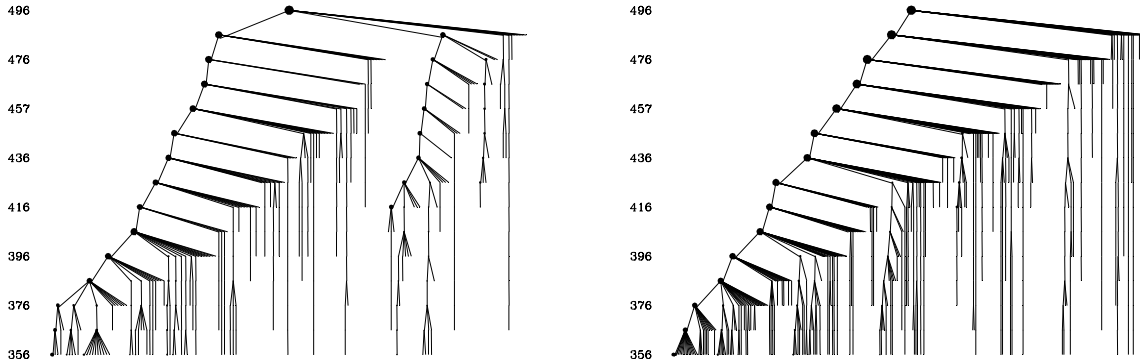


Figure 1. Illustrative merger trees for two halos with masses of 1.2 (left) and $2.9 \times 10^{10} h^{-1} M_{\odot}$ (right). Time runs upwards in steps of 10 Myr, from $z = 12.7$ (bottom) to $z = 10$ (top) and the age of the Universe (in Myr) is shown at every second step. At each time the area of the symbol is proportional to the halo mass, with masses decreasing to the right in each group, and lines show the progenitor relationship. The leftmost branch shows the main trunk of the tree. The halo at left has a (major) 1:2 merger at the last time step, while the main trunk of halo at right has a 1:2 merger at the first time step, a 1:6 two steps later and then only smaller mergers after that.

gains and the comparison to Press-Schechter. The consequences of this merging in a simple model for photon production are elucidated in §4 and we summarize and conclude in §5.

2 SIMULATIONS AND PARAMETERS

We base our conclusions on 5 dark matter only N-body simulations of a Λ CDM cosmology with $\Omega_m = 0.25$, $\Omega_{\Lambda} = 0.75$, $h = 0.72$, $n = 0.97$ and $\sigma_8 = 0.8$, in agreement with a wide array of observations. The initial conditions were generated at $z = 300$ using the Zel’dovich approximation applied to a regular, Cartesian grid of particles. Our two highest resolution simulations employed 800^3 equal mass particles ($M = 2 \times 10^6$ and $1.7 \times 10^7 h^{-1} M_{\odot}$) in boxes of side 25 and $50 h^{-1}$ Mpc with Plummer equivalent smoothings of 1.1 and $2.2 h^{-1}$ kpc. They were evolved to $z = 10$ using the *TreePM* code described in White (2002) (for a comparison with other codes see Heitmann et al. 2007). We ran 3 additional, smaller simulations in a $20 h^{-1}$ Mpc box, one with 600^3 particles and two with 300^3 particles (each started at $z = 200$). A comparison of the boxes allows us to check for finite volume, finite mass and finite force resolution effects. We shall comment on each where appropriate.

The phase space data for the particles were dumped at 15 outputs spaced by 10 Myr from $z = 12.7$ to $z = 10$ for all but the largest box. The lower resolution of the largest box makes it less useful for merger trees, so it was sampled for only subset of these output times, ending at $z = 10$. For each output we generate a catalog of halos using the Friends-of-Friends (FoF) algorithm (Davis et al. 1985) with a linking length, b , of 0.168 times the mean inter-particle spacing. This partitions the particles into equivalence classes, by linking together all particle pairs separated by less than b . The halos correspond roughly to particles with $\rho > 3/(2\pi b^3) \simeq 100$ times the background density. We also made catalogs using a linking length of 0.2 times the mean inter-particle spacing, which we shall discuss further below. We found that the FoF algorithm with a larger linking length had a tendency to link together halos

which we would, by eye, have characterized as separate (see also Davis et al. 1985; Cole & Lacey 1996, for similar discussion). This problem is mitigated with our more conservative choice of b .

For each halo we compute a number of properties, including the potential well depth, peak circular velocity, the position of the most bound particle (which we take to define the halo center) and M_{180} , the mass interior to a radius, r_{180} , within which the mean density is 180 times the background density². As discussed in White (2001, 2002) and Hu & Kravtsov (2003), the choice of halo mass is problematic and ultimately one of convention. We shall return to this issue in the next section.

Merger trees are computed from the set of halo catalogs by identifying for each halo a “child” at a later time. The child is defined as that halo which contains, at the later time step, more than half of the particles in the parent halo at the earlier time step (weighting each particle equally). For the purposes of tracking halos this simple linkage between outputs suffices (note that we do not attempt to track sub-halos within larger halos, which generally requires greater sophistication). Two examples of the halo merger trees are given in Fig. 1, where we see a rich set of behaviours, including major and minor mergers and many body mergers. From the merger trees it is straightforward to compute the time when a halo ‘falls in’ to a larger halo, the number and masses of the progenitors etc.

Due to finite computational resources, all N-body simulations must trade-off computational volume for mass resolution. By running multiple simulations we can overcome this to some extent, but not entirely. We have chosen to slightly under-resolve the low mass ($T_{\text{vir}} \simeq 10^4 \text{K}$) halos in order to simulate a slightly larger volume, since our focus

² Note this is simply a definition of halo mass, not the halo finder. We still use FoF particles to define the group centers. However given the center we use all of the particles in the simulation when determining M_{180} . Our M_{180} masses should thus be comparable to the sum of the particles in an $SO(180)$ group – a common definition that employs both the $SO(180)$ halo finder and definition of mass.

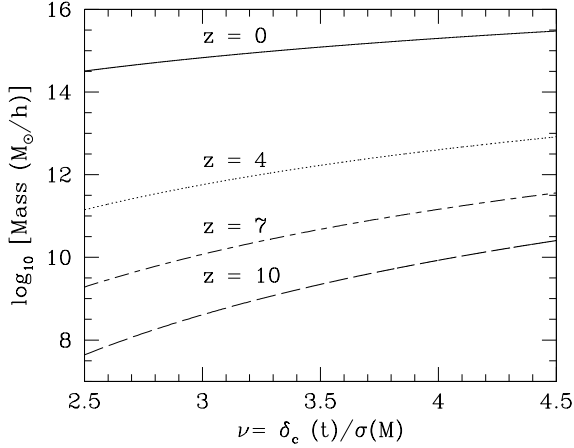


Figure 2. The peak height, ν – which governs the abundance, clustering and merging behavior in analytic models – for $z = 0, 4, 7$ and 10 . For example, objects with $\nu = 3$ have $M \simeq 4 \times 10^8 h^{-1} M_\odot$ at $z = 10$ but $M \simeq 6 \times 10^{14} h^{-1} M_\odot$ at $z = 0$.

will be on the more massive halos which have more frequent major mergers. Under reasonable assumptions (see below) between $\frac{1}{3} - \frac{2}{3}$ off all photon production occurs in halos more massive than $10^9 h^{-1} M_\odot$ at $z = 10$, and we easily resolve these objects with the $25 h^{-1} \text{Mpc}$ simulation which we use for the bulk of the paper.

3 HALO PROPERTIES

3.1 Halo abundance and clustering

The highest mass objects in our volume have mass $\sim 10^{10} h^{-1} M_\odot$ and radii of several tens of kpc. At $z = 10$ these halos are analogous to rich clusters today, being recently formed and rare: Fig. 2 shows the mass as a function of peak height, $\nu \equiv \delta_c/\sigma(M)$, at $z = 10, 7, 4$ and 0 . The threshold $\delta_c(t)$ is defined as $1.686/D(t)$, where D is the linear growth factor normalized to unity at $z = 0$ and $\sigma^2(M)$ is the variance of the mass computed using linear theory at $z = 0$. In our cosmology $\delta_c(z = 10) \simeq 13.8$. Due to the flatness of the dimensionless power on the scales of interest, the slightly red initial spectrum and the low clustering amplitude, the characteristic mass, M_* , where $\sigma \sim \delta_c$, is $\mathcal{O}(1) M_\odot$ at $z = 10$, so all of the halos we consider are $\gg M_*$.

One of the most basic and useful quantities we can derive from the simulations is the mass function, the spatial abundance of halos as a function of mass. High redshift mass functions have been studied by many groups (e.g. Jang-Condell & Hernquist 2001; Reed et al. 2005; Springel et al. 2005; Reed et al. 2007; Heitmann et al. 2006; Trac & Cen 2006; Iliev et al. 2005, 2006a; Maio et al. 2006; Zahn et al. 2007; Lukic et al. 2007) and Lukic et al. (2007) offer a comprehensive summary of recent work. Most previous work finds mass functions which are better fit by the Sheth & Tormen (1999), Jenkins et al. (2001) or Warren et al (2005) form. We find that the appropriate mass function to use depends primarily on the definition of mass chosen and definitions which at $z \simeq 0$ give very similar mass functions can give quite different ones at $z = 10$.

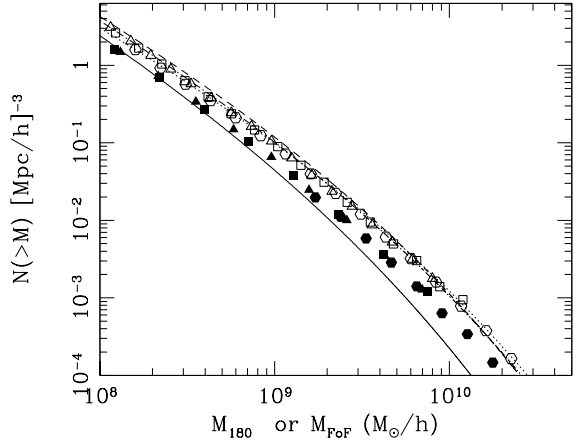


Figure 3. The mass functions for our box compared to the Warren et al (2005) (dashed line), Jenkins et al. (2001) (dash-dotted line), Sheth & Tormen (1999) (dotted line) and Press-Schechter (solid lower line) mass functions for our cosmology. N-body M_{180} results are plotted as solid symbols for the 800^3 ($25 h^{-1} \text{Mpc}$, squares, $50 h^{-1} \text{Mpc}$, hexagons) and 600^3 ($20 h^{-1} \text{Mpc}$, triangles) runs. Only masses where there are more than 10 halos in the box and where resolution effects are unimportant are shown. Open symbols denote the analogous FoF(0.2) mass functions for the same simulations.

We show the mass function(s) from our three highest resolution simulations in Fig. 3. If we use as our mass estimator the sum of the particle masses in the FoF(0.2) groups (open symbols) then we find good agreement with the Sheth & Tormen (1999) or Jenkins et al. (2001) forms. This is the procedure followed by most of the groups above³. However if we choose instead to use M_{180} as our mass estimator (filled symbols) we find a different mass function. Although this mass function shows a marked excess of high mass halos compared to the Press & Schechter (1974) form, it is a better fit than the alternate forms mentioned above. Agreeably, for the scales plotted, the M_{180} mass function is independent of the initial FoF group catalog used to define the centers about which M_{180} is determined. This is not too surprising as the group centers hardly change and the number of “small” groups which split off of larger FoF groups as the linking length is decreased is tiny compared to the number of low-mass “field” halos. The differences in mass functions then comes primarily from the definition of the masses of the found objects. Comparing halo by halo the FoF(0.2) masses are almost twice M_{180} , though the difference depends on mass. A similar difference was also noted by Reed et al. (2007) as a shift to lower abundance at fixed mass when comparing an FoF(0.2)-based mass function to that of a different halo finder. We believe the primary is-

³ Due to the finite size of our boxes the mass function is slightly suppressed at high mass. We can estimate this suppression using (extended) Press-Schechter theory, assuming we have simulated the conditional mass function within a region of exactly mean density on the mass scale of the box. The mass functions plotted have been corrected for this expected suppression, which ranges from $< 1\%$ to 22% over the mass range plotted. See, e.g. Lukic et al. (2007); Reed et al. (2007) for further discussion.

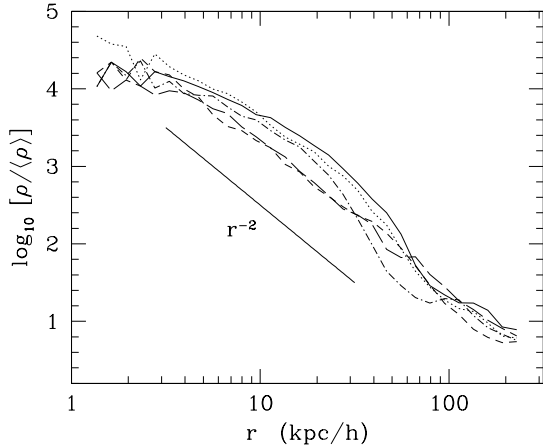


Figure 4. Density profiles of the 5 most massive halos in the 800^3 run at $z = 10$. The masses range from $1 - 3 \times 10^{10} h^{-1} M_{\odot}$. The 2 halos with the flatter profiles (short and long dashed lines) correspond to the 3rd and 4th most massive halos and both have had a major merger (greater than 1:6) within the previous 10 Myr. Halo sizes (r_{180}) are below $100 h^{-1} \text{kpc}$ for all of the halos shown. The solid line, offset, shows an isothermal sphere profile ($\rho \propto r^{-2}$) for comparison. This indicates why FoF(0.2) masses assuming an isothermal profile may be expected to disagree with SO(180) masses as discussed in the text.

sue is not the halo finder, but the mass definition. Their second halo finder assigns masses which are essentially our M_{180} . The mass discrepancy is much larger for these halos at $z = 10$ than it is for group and cluster-sized halos at the present day (e.g. Figure 11 in White 2002).

The mass differences are quite interesting. The historical argument for choosing FoF(0.2) was that the FoF group finder selects particles approximately within a density $3/(2\pi b^3) \simeq 60$ times the mean density. For a singular isothermal sphere profile ($\rho \propto r^{-2}$) and a critical density Universe the mean enclosed density is thus $180 \rho_{\text{crit}}$, in accord with arguments based on spherical top-hat collapse (e.g. Peacock 1998). At $z = 10$ the Universe is close to critical density so we might expect the FoF(0.2) and M_{180} mass functions to agree better than at lower z where $180\bar{\rho} \simeq 45\rho_{\text{crit}}$. However, we are focusing on very high mass halos which have only recently formed at $z = 10$. They are therefore less centrally concentrated⁴ than a ‘typical’ halo. This can also be seen in Fig. 4, where halo profiles are compared to the isothermal sphere profile. As the halo profiles are less steep than the isothermal sphere form assumed in the argument above, this leads to the differences in mass between the FoF(0.2) and SO(180) definitions.

By contrast, we find that the FoF(0.168) mass function is very similar to the M_{180} points plotted, and a halo by halo comparison shows that the two masses agree to within 20-30 per cent. As we go down the mass function, to more concentrated, lower mass halos, we expect FoF(0.2) to better match M_{180} (e.g. Cole & Lacey 1996).

In general, given the strong dependence of the mass

⁴ They correspond roughly to $c \simeq 2 - 5$ for halos of the form proposed by Navarro, Frenk & White (1997).

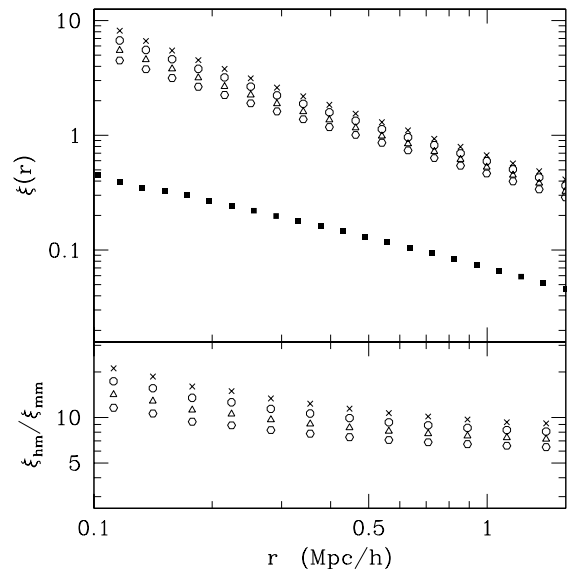


Figure 5. (Top) The halo-dark-matter cross correlation, $\xi_{hm}(r)$ (top), for halos with (comoving) number density $10^{-2.0}$, $10^{-1.5}$, $10^{-1.0}$ and $10^{-0.5} h^3 \text{Mpc}^{-3}$ (open symbols from top to bottom) from our $50 h^{-1} \text{Mpc}$ simulation. The solid squares show the dark matter correlation function, $\xi_{mm}(r)$. The ratio, $b(r) \equiv \xi_{hm}(r)/\xi_{mm}(r)$, is shown in the lower panel.

function upon the mass definition, and the ambiguity in this quantity in many analytic treatments, significant care must be taken when making predictions for the abundance of halos. Even if we decide to treat all halos as a simple 1-parameter family, it is likely preferable to make comparisons with some quantity more directly related to observables (such as circular velocity, halo virial temperature or potential well depth) or to discuss statistics as a function of number density rather than mass.

Like rich clusters we expect that these massive halos, in the process of formation, will not lie on the usual ‘vacuum’ virial relation $2\text{KE}=\text{PE}$, where KE and PE refer to the potential and kinetic energy respectively. In fact we find that $2\text{KE}/\text{PE} \simeq 1.4$ for halos in the range $10^8 - 10^{10} h^{-1} M_{\odot}$, very similar to the value found for rich clusters today (Knebe & Muller 1999; Cohn & White 2005; Shaw et al. 2007). A similar ‘excess’ kinetic energy was also found by Jang-Condell & Hernquist (2001) for lower mass halos. The ratio is larger than unity because of the steady accretion of material onto the cluster (Cole & Lacey 1996).

Fig. 5 shows the clustering of the dark matter and the halos from our $50 h^{-1} \text{Mpc}$ run. We plot the auto-correlation function of the dark matter and the cross-correlation of the halo centers with the dark matter respectively. The latter is both less subject to noise⁵ from our small sample of massive halos and more applicable to understanding how radiation from the halos would influence the surrounding mass. The

⁵ There is essentially no shot-noise for the dark matter, $\xi_{mm}(r)$, and jackknife errors on the cross-correlation, ξ_{hm} , are a few per cent for the samples shown. Jackknife drastically underestimates the errors from finite volume however.

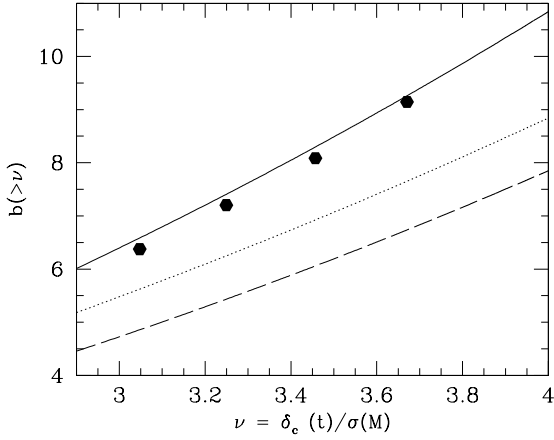


Figure 6. A comparison of the large-scale bias measured for the mass thresholded samples of Fig. 5 with a number of theoretical models: the bias of the Press-Schechter mass function (as computed by Efstathiou et al. 1988; Cole & Kaiser 1989, solid), the Sheth-Tormen mass function (Sheth & Tormen 1999, dashed) and the fitting function of Sheth, Mo & Tormen (2001, dotted). Although the mass function is in good agreement with that of Sheth & Tormen (1999), their bias formula underestimates the clustering of the rarest halos.

ratio of the cross- to auto-correlation functions defines the scale dependent bias, $b_h(r)$.

The mass auto-correlation function is in good agreement between the 25 and 50 h^{-1} Mpc boxes up to 1 h^{-1} Mpc, with ξ from the 25 h^{-1} Mpc box falling below that of the 50 h^{-1} Mpc box beyond this scale. The 20 h^{-1} Mpc box has noticeably less power over a wide range of scales. For the masses where we can compare and for the range of linear scales plotted, the halo-mass cross-correlation functions of the 25 and 50 h^{-1} Mpc boxes are in excellent agreement, so we have shown the results only for the 50 h^{-1} Mpc box.

Our halo samples are mass thresholded, however by using number density as our marker we largely avoid the issues of mass definition discussed earlier. The differences in bias at fixed \bar{n} for the different mass choices, arising from the scatter between different mass definitions, is only a few percent. Taking $b_h(1.5 h^{-1}\text{Mpc})$ as the asymptotic value, the large-scale bias is in good agreement with the models of Press & Schechter (1974); Efstathiou et al. (1988); Cole & Kaiser (1989); Mo & White (1996); Jing (1998) and $\sim 30\%$ higher than that of Sheth & Tormen (1999). Those of Sheth, Mo & Tormen (2001) and Tinker et al. (2005) lie in between. (The model of Seljak & Warren (2004) only extends up to 100 times the non-linear mass, where $b \sim 3$, and it not applicable to our results.) To make contact with the earlier literature we plot in Fig. 6 the bias as a function of peak height, ν , obtained from \bar{n} using the Sheth & Tormen (1999) mass function. When computing $b(>\nu)$ in the simulation we rank order the halos by FoF(0.2) mass in order to best match the chosen mass function. This mass function is then used when analytically computing the halo-weighted bias $b(>\nu)$ from each of the analytic forms which provide $b(\nu)$. Because of this the Sheth & Tormen (1999) bias function is the only one which would give an average bias of unity when integrated over ν .

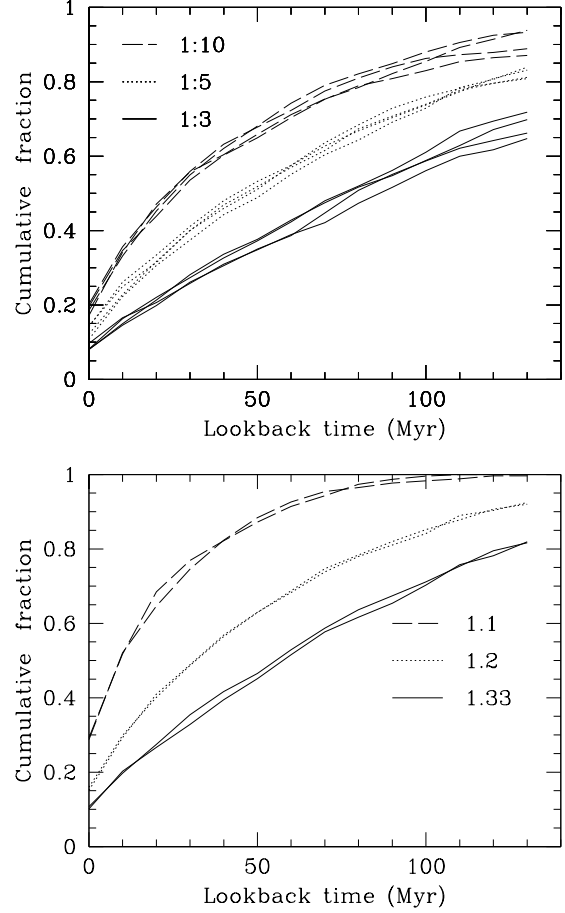


Figure 7. (Top) The fraction of halos with $M > 10^9 h^{-1}M_\odot$ which have had a 1:10, 1:5 or 1:3 merger (top to bottom) back to the lookback time shown in all 4 of our simulations. (Bottom) The fraction of halos with $M > 10^9 h^{-1}M_\odot$ which have a large mass gain ($m_f/m_i \geq 1.1, 1.2, 1.33$) vs. time. Here we show only the two highest resolution simulations for clarity. Both plots would coincide if all mergers were 2-body within 10 Myr.

Similar trends for rare halos to have larger bias than the modern fits predict have been seen at lower redshift (e.g. Shen et al. 2008; White, Martini & Cohn 2008; Angulo, Baugh & Lacey 2008, for recent work) but we must also remember that $b_h(1.5 h^{-1}\text{Mpc})$ is likely higher than $b_h(r \rightarrow \infty)$ so the degree of overshoot is hard to quantify precisely. As expected, the clustering strength is an increasing function of mass (Kaiser 1984; Efstathiou et al. 1988; Cole & Kaiser 1989), or a decreasing function of halo abundance.

3.2 Mergers and Mass Gains

We now consider the hierarchical assembly of the dark matter halos through merging and accretion. We shall use the $800^3, 25 h^{-1}\text{Mpc}$ simulation since it provides both high mass resolution and a representative volume. Since our progenitor relationships are based on particles in the FoF groups, we use the FoF(0.168) masses for consistency. As discussed earlier, for our massive halos these masses are within 20–30

per cent of M_{180} and none of our conclusions depend sensitively on this choice. Fig. 7 shows the fraction of halos with $10^9 \leq M \leq 10^{10} h^{-1} M_\odot$ which have experienced at least one major merger as function of lookback time, in intervals of 10 Myrs. We show three different definitions of ‘major’ merger, where the largest two progenitors of the halo have ratios below 1:10, 1:5 or 1:3. Mergers are frequent but not ubiquitous – not all halos have had a major merger within 140 Myrs, but many have. The fraction decreases for smaller mass ratios and for lower mass halos, as expected.

We can also consider mass gains between time steps, often denoted in the literature as m_f/m_i where m_i is the mass of the largest progenitor at the earlier time and m_f is the mass of the halo under consideration. Mass gains are sometimes used as a proxy for mergers. Fig. 7 shows those halos whose mass increased by at least 10, 20 or 33 per cent as a function of lookback time. The top and bottom panels of Fig. 7 would be identical if all mergers were two body and there was no smooth accretion. As can be seen in Fig. 1 this is not the case; Fig. 7 quantifies this difference for major mergers.

The Press-Schechter model predicts the evolution of the mass function, and it can be extended to make predictions for the time history of halos. This “excursion set formalism” is often called extended Press-Schechter (Bond et al. 1991; Bower 1991; Lacey & Cole 1993, 1994; Kitayama & Suto 1996) and denoted EPS – see Zentner (2006) for a recent review. Although it is analytically tractable, it has many inconsistencies and does not compare particularly well to N-body simulations (see e.g. Sheth & Pitman 1997; Tormen 1998; Somerville et al. 2000; Cohn, Bagla & White 2001; Benson, Kamionkowski & Hassani 2005; Li et al. 2006). For example, Li et al. (2006) found that with EPS halos of mass $10^{11} - 10^{14} h^{-1} M_\odot$ at $z \simeq 0$ formed later than in N-body simulations (but see Percival, Miller & Peacock 2000, for a slightly different quantity). In Fig. 8 we compare the N-body mass accretion histories for massive halos at $z = 10$ to a model by Miller et al. (2006) based on EPS which predicts almost exponential growth with redshift. (Other analytic models also exist, see e.g. Neistein, van den Bosch & Dekel (2006) for a summary and comparison, there are some discrepancies between these which are not yet fully understood.) We find that EPS predicts mass growth which is too rapid also for the high mass, high redshift regime studied here. The N-body mass accretion histories *are* relatively well fit by an exponential in z – a growth model also proposed by Wechsler et al. (2002) on the basis of N-body simulations of galaxy-sized halos at low z – but the coefficient predicted by Miller et al. (2006) is larger than measured in the simulations.

Perhaps the most common use of EPS is to predict merger rates, and EPS has been used in this context in several recent models of reionization. To compare the EPS predictions with our simulations we computed merger rates using only our last (10 Myr) time step, taking for any halo with $z = 10$ mass within M_f to $M_f + \Delta M_f$ the distribution of progenitors⁶, M_{prog} . The EPS prediction can be found in the Appendix.

⁶ We thank D. Holz for suggesting this as a useful comparison quantity.

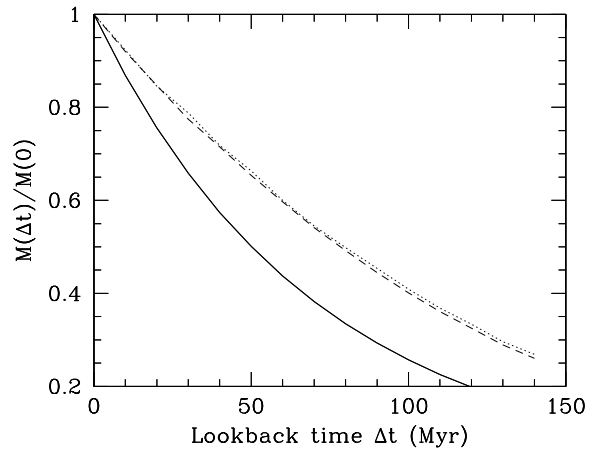


Figure 8. The mass accretion history for halos in the range $(5 - 8) \times 10^8 h^{-1} M_\odot$ from the 800^3 (dashed) and 600^3 (dotted) simulations and the functional form of Miller et al. (2006, solid) based on EPS.

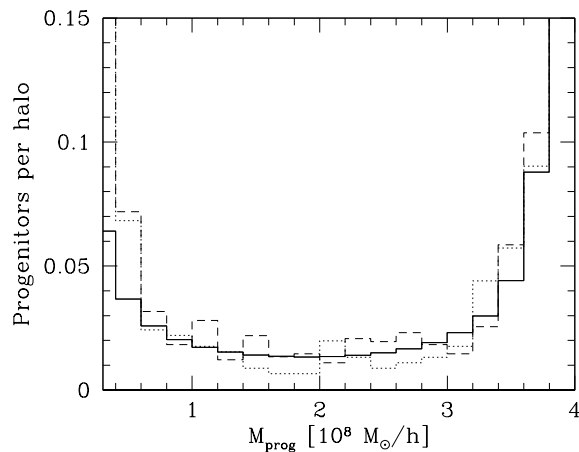


Figure 9. EPS (solid) and simulation (dotted and dashed) results for the number of progenitors of halos with $M_f = (4 - 4.5) \times 10^8 h^{-1} M_\odot$ as a function of M_{prog} .

We show a representative example of $N(M_{\text{prog}})/N(M_f)$ for M_f in the range $(4 - 4.5) \times 10^8 h^{-1} M_\odot$ in Fig. 9. For most of the range the agreement is reasonably good. At the low mass end EPS significantly underpredicts the number of predecessors found in our simulations (see also Percival 2001). At the high mass end the EPS rate starts to climb rapidly, eventually diverging unphysically. These trends are independent of the final mass chosen, or the definition of mass used. The EPS formula as progenitor mass goes to zero also diverges, which we could not approach due to our finite mass resolution, but the mass weighted EPS calculation is finite at both ends⁷. There is another notable difference between EPS and our simulation. Though it is relatively small, our time step is still too large for all mergers to be truly 2-body (see Fig. 1), as implicitly assumed by EPS. A large fraction

⁷ We thank Jun Zhang for emphasizing this.

(20-50 per cent, depending on M_f) of the halos are actually produced in 3 (or more)-body mergers.

Finally we also looked for evidence that recently merged halos clustered differently than randomly chosen halos of the same mass. The correlation function of 1:2 or 1:3 mergers appeared to be slightly ($< 10\%$) enhanced at 1 Mpc compared to the random sample, but the number of merged halos was too small for this to be statistically meaningful. The effect thus appears to be modest, if present at all, just as was found for lower redshift, high-mass halos (e.g. Gottlöber et al. 2002; Percival et al. 2003; Scannapieco & Thacker 2003; Wetzel et al 2007). This suggests that the clustering of massive halos does not depend strongly upon their recent merger history. This in turn significantly eases the modeling of merger-related processes, such as enhanced photon production during reionization which we now discuss.

4 REIONIZATION EFFECTS

The rate of photon production in a galaxy can be enhanced by mergers, which can trigger starbursts or possibly accretion onto a black hole which may be present (e.g. Carlberg 1990; Barnes & Hernquist 1991, 1996; Mihos & Hernquist 1994, 1996; Kauffmann & Haehnelt 2000; Cavaliere & Vittorini 2000). It is reasonable to anticipate that the mergers of large dark matter halos could have similar effects on the photon production rate of the sources within them. We will make this assumption, and then consider the consequences of the merger rates computed above for the photon production distribution.

We frame our discussion in terms of a simple but promising model for reionization proposed by Furlanetto, Zaldarriaga & Hernquist (2004b), though our result is true more generally. In these models, a halo of a given mass m (in units of some reference mass) is considered a source of photons with rate

$$\frac{dn_\gamma}{dt} = \zeta_t(m)m \quad . \quad (1)$$

Usually ζ_t is taken to be mass independent, scale as $m^{2/3}$ or transition from $m^{2/3}$ to m^0 at $M \sim 10^{10} h^{-1} M_\odot$ (Furlanetto, McQuinn & Hernquist 2005, motivated by Kauffmann et al. 2003). A region around these halos is taken to be ionized if the photons within it are sufficient to ionize all the interior mass. Some extensions also give recombinations spatial and/or temporal dependence and incorporate this into finding the bubble properties (Furlanetto & Oh 2005; Furlanetto, McQuinn & Hernquist 2005; Cohn & Chang 2007), or incorporate Eq. (1) into N-body simulations (Iliev et al. 2006a; McQuinn et al. 2007; Zahn et al. 2007). Under these assumptions the morphology of ionized regions can be computed from the photon production rate and spatial distribution of dark matter halos.

A first step at including halo mergers within the above formalism (and its generalizations) was presented in Cohn & Chang (2007). Those calculations were based on the Press-Schechter formalism, and so could only provide average numbers of mergers for halos in a given mass range; scatter was computed by assuming that the mergers had a Poisson distribution. With our simulations we are able to

check these assumptions and significantly extend this work because we have access to the detailed merger history of each halo. This allows us to go beyond their analytic estimates to explicitly calculate the full distribution of photon production for a halo of mass m , taking into account the distribution of histories and their associated (and different) photon production rates for a fixed m .

From the merger tree for each halo at $z = 10$ ($t = t_{\text{obs}}$) we identify which progenitors had at least one major merger (greater than 1:3 or 1:10), and the time t_{merge} they occurred. We include all of the mergers in the tree and we place t_{merge} at random within the 10 Myr interval between the relevant outputs. Each of these mergers is allowed to contribute “excess” photons beyond those which would automatically be assigned to the halo on the basis of its $z = 10$ mass, M_h , but the number of photons contributed is exponentially attenuated with an e -folding time τ . The “excess” photon production is thus proportional to

$$\mathcal{M}_s^\alpha \equiv \sum_{\text{merge}} M^\alpha e^{(t_{\text{merge}} - t_{\text{obs}})/\tau} \quad , \quad (2)$$

where the sum is over all halos which have undergone a major merger and we take $\alpha = 1$ or $5/3$. The exponential decay is motivated by modeling of starbursts, e.g. Conselice (2006), hence the subscript s . We also consider another variant, including all halos with major mergers within τ of t_{obs} , with no attenuation:

$$\mathcal{M}_{bh} \equiv \sum_{\text{merge}} M \Theta(t_{\text{obs}} - t_{\text{merge}} - \tau) \quad , \quad (3)$$

where $\Theta(x) = 1$ if $x > 0$, $1/2$ if $x = 0$ and zero otherwise. We denote this by a subscript bh , to indicate photon production by black holes, which might have their photon production rate increase over time and then decay once the fuel is exhausted. Assuming a step-like function is a crude first approximation to this uncertain physics. In all cases we take the quiescent photon production to depend on the $z = 10$ halo mass with the same index, α , as \mathcal{M}_s . We note this prescription might cause some overcounting if many mergers occur within a short time period and the gas becomes depleted from the earliest ones. A more refined model would account for the evolving baryon budget within the halo, but our treatment is sufficient for the purpose of illustration.

The relative amplitudes of these two modes of photon production depend on a number of different factors (see e.g. Cohn & Chang (2007) for discussion and summary of estimates at these redshifts) but a factor $\beta \sim 5$ is not unreasonable for starbursts and could be even larger for black holes. The total photon production is thus enhanced by a factor

$$\epsilon_{\text{mrg}} \equiv \frac{M_h^\alpha + \beta \mathcal{M}_s^\alpha}{M_h^\alpha} \quad (4)$$

for the “starburst” prescription, or its analogue $\mathcal{M}_s^\alpha \rightarrow \mathcal{M}_{bh}$ for the “black hole” prescription. In principle both can contribute. We considered the two effects separately, their combination is straightforward.

Figure 10 shows a typical example of the cumulative distribution of enhancement factors, Eq. (4). We took the starburst form, 1:3 mergers, $\alpha = 5/3$, $\tau = 75$ Myr and $\beta = 5$, but other cases are very similar. The enhancement distribution is extended, with a long tail to high ϵ_{mrg} and a peak at those halos which have not merged. About half of the halos

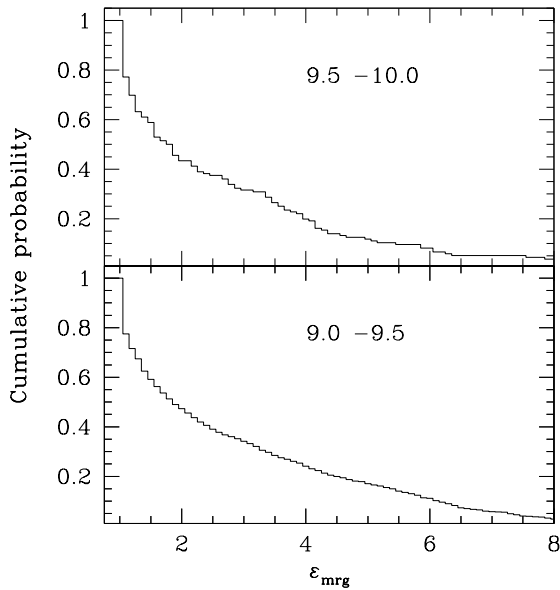


Figure 10. The cumulative probability for enhancement of photon production over the quiescent case, ϵ_{mrg} , for one toy model. In this example, mergers (1:3) enhance the quiescent photon production rate ($\sim m^{5/3}$) at $z = 10$ with $\beta = 5$ and $\tau = 75$ Myr (see text). Roughly 80 per cent of these halos have some enhancement, shown for 2 bins in halo mass (with the range in $\log_{10}(M/h^{-1}M_{\odot})$ shown in each panel). There are 1195 and 136 halos in the low- and high-mass bins, respectively. The peak at $\epsilon_{\text{mrg}} = 1$ comes from the 20 per cent of the halos which have had no 1:3 mergers in the previous 140 Myr. Trends for other parameters and parameterizations are discussed in the text.

have twice the photon production, while 20 per cent have no enhancement. Choosing a larger β increases the size of the enhancement, but does not qualitatively change the form of the distribution. Similarly, changing α or τ changes the detailed form of the distribution but not its character. Halos down to $10^8 h^{-1}M_{\odot}$ show a very similar distribution of enhancements. By contrast the model for black hole accretion produces a bimodal distribution, as the “early” mergers contribute relatively more than in the case of the starbursts, leading to a second peak.

Even though the scatter in photon contributions from halo to halo is large for a given mass, if a large number of such halos are found in a bubble, their contributions to the photon numbers will tend to the mean, allowing the distribution to be replaced by the average. Precisely counting the number of halos of a given mass and the combined photon scatter inside a typical bubble is unfortunately self-referential: changing the ionization properties (including mergers) changes the bubble sizes and thus the number of halos within. Different assumptions about the nature of the sources and their feedback can give drastically different bubble sizes, and the relative importance of high vs. lower mass halos (e.g. McQuinn et al. 2007; Zahn et al. 2007). Given these uncertainties we consider properties in an average volume, for illustration.

For quiescent photon production and $\zeta \propto m^{2/3}$, analytic estimates such as Press-Schechter give that halos with $M > 10^9 h^{-1}M_{\odot}$ contribute between $\frac{1}{3} - \frac{2}{3}$ of all pho-

tons. Even choosing $\zeta \propto m^0$, such halos contribute ~ 10 per cent of the photons. The number density of such halos is $\sim 0.03 h^3 \text{Mpc}^{-3}$. Bubble radii in different models range over several orders of magnitude. A middle-of-the-road estimate is $3 h^{-1} \text{Mpc}$, which would contain about 3 halos with $M > 10^9 h^{-1}M_{\odot}$. The bubble radius would also be larger than the correlation length of our halos, so clustering is only expected to change this number by a factor of order unity. A small number of halos contributing a large fraction of the photons means that scatter in their photon production should affect the properties of the bubbles.

Our calculation is relatively crude, but it suggests that the inclusion of mergers into a more refined model of reionization could alter the distribution of ionized regions. For models based on approximate dynamics (e.g. McQuinn et al. 2007; Mesinger & Furlanetto 2007; Zahn et al. 2007), a possible first step would be to assign a merger history to the sources at random. This is accurate to the extent that recently merged halos are not spatially biased with respect to a random sample of halos of the same mass. For models which marry the analytic model to dark matter simulations⁸ the merger history is known, so only the photon production rate needs to be modified. More complex simulations involving radiative transfer will need to follow the photon production history as the halos evolve, perhaps using a semi-analytic model (such as in Benson, et al. 2001; Ciardi, Stoehr & White 2003; Benson, et al. 2006). A full-blown simulation including radiative transfer and N-body in a large enough volume is still out of reach (but see Sokasian et al. 2003; Kohler, Gnedin & Hamilton 2005; Trac & Cen 2006; Iliev et al. 2006a,b, for recent progress).

5 SUMMARY AND CONCLUSIONS

Using 5 N-body simulations with different sized boxes and particle loads we considered the abundance, clustering and assembly histories of high mass halos at high redshift. We present results specifically for $z = 10$, but the evolution of the populations is smooth and the results will be similar at slightly higher and lower redshift. Like the halos of rich groups or clusters today the halos we consider are in the process of forming, growing rapidly through accretions and mergers. We found that they had larger velocity dispersions than a naive application of the virial theorem would predict, due to a surface pressure from infalling material. Being recently formed, the halos were not very centrally concentrated, leading to a factor of two difference between FoF(0.2) masses and M_{180} . When measured against M_{180} we found our halo abundances were closer to the Press-Schechter fitting formula than that of Sheth & Tormen (1999), though the simulations had more high mass halos than the analytic form. If FoF(0.2) masses were used instead, the mass function approached that of Sheth & Tormen (1999), in agreement with earlier work. This discrepancy indicates that analytic models which assign an observable to halos of a given size need to pay particular attention to the marker of halo size employed.

⁸ Unfortunately our simulation volumes are too small to provide converged answers for this step with the existing runs.

The high mass halos were significantly clustered, and we calculated the halo bias by taking the halo-mass cross correlation and dividing by the matter auto-correlation function. Our rare halos were more clustered than the recent models of Sheth & Tormen (1999); Sheth, Mo & Tormen (2001); Tinker et al. (2005) and closer to the models of Efstathiou et al. (1988); Cole & Kaiser (1989); Mo & White (1996); Jing (1998).

Merging is common, though not ubiquitous, in high mass halos at $z = 10$. Major mergers, with progenitor mass ratios less than 1:3, occurred within 140 Myr of $z = 10$ for more than half of halos with $M > 10^9 h^{-1} M_\odot$. We looked at the fraction of halos undergoing mergers for a variety of lookback times and progenitor ratios, finding more mergers for more massive halos, longer lookback times or less extreme merger events. Mass gains, parameterized by m_f/m_i , showed similar trends even though not all merger events were two body within our 10 Myr time step. The EPS model provides a reasonable description of the progenitor mass distribution, though it underpredicts the number of low mass progenitors and diverges as $M_{\text{prog}} \rightarrow M_h$. The mass accretions histories predicted by EPS, as calculated by Miller et al. (2006), provide only a qualitative guide to the mean mass accretion histories seen in our simulations.

At $z = 10$ reionization is expected to be underway due to photon production from astrophysical objects which formed in collapsed halos. Within the context of a simple model which associates mergers with an increase in photon production rate the photon production distribution developed a high rate tail due to recently merged halos. Including these photon production enhancements will likely drive scatter in photon production at fixed halo mass. Since the number of massive halos within a typical ionized bubble can be small, this scatter in photon production could well translate into additional scatter in bubble sizes and it would be very interesting to include this effect in approximate models of reionization. If the recently merged halos are not spatially biased with respect to other halos of the same mass, including these effects in models, even those without merger trees, should be straightforward.

JDC would like to thank D. Holz and S. Koushiappas for conversations. We thank O. Zahn for helpful comments on an early draft, and S. Furlanetto, C.P. Ma, L. Miller, E. Neistein and J. Zhang for comments on the final draft. The simulations were analyzed on the supercomputers at the National Energy Research Scientific Computing center. MW was supported by NASA. We thank the referee for encouraging us to run the $50 h^{-1} \text{Mpc}$ box.

APPENDIX

We compared the progenitor mass distribution from the simulations with the predictions of the extended Press-Schechter formalism. To compute the distribution in this formalism we need the number of progenitors with $m_{i1} < m_i < m_{i2}$ at time $t - \Delta t$ for a given range of final masses, $m_{f1} < m_f < m_{f2}$, at time t . The EPS theory gives

$$\frac{N(m_{\text{prog}}, \Delta t)}{\Delta t} = \int_{m_{f1}}^{m_{f2}} dM N(M, t) \int_{m_{i1}}^{m_{i2}} dM_i \times (M/M_i) \dot{P}_1(M_i \rightarrow M, t) \quad (5)$$

where the number of halos of mass M , $N(M, t)$, is given by the usual mass function (Press & Schechter 1974):

$$N(M, t) = \frac{1}{\sqrt{2\pi}} \frac{\rho_0}{M} \frac{\delta_c(t)}{\sigma^3(M)} \left| \frac{d\sigma^2}{dM} \right| \exp \left[-\frac{\delta_c^2(t)}{2\sigma^2(M)} \right] \quad (6)$$

with ρ_0 the background density. To get Eq. (5) the number of halos at a given time is multiplied by the fraction of halos that have mass M at t and have jumped from mass M_i within δt :

$$(M/M_i) \dot{P}_1(M_i \rightarrow M; t) dM_i \delta t = (M/M_i) (2\pi)^{-1/2} (\Delta\sigma^2)^{-3/2} \left[-\frac{d\delta_c(t)}{dt} \right] \left| \frac{d\sigma^2(M_i)}{dM_i} \right| dM_i \delta t. \quad (7)$$

where $\Delta\sigma^2 = \sigma(M_i)^2 - \sigma(M)^2$. To produce the EPS predictions discussed in §3.2, we take $\delta t = \Delta t = 10$ Myr, assuming that this time is small.

REFERENCES

- Angulo, R.E., Baugh, C.M., Lacey, C.G., 2008, preprint [arxiv/0712.2280]
 Barkana, R., 2007, MNRAS 376, 1784
 Barkana, R., Loeb, A., 2001, Phys. Rep., 349, 125
 Barnes, J.E., Hernquist, L., 1991, ApJ, 370, L365
 Barnes, J.E., Hernquist, L., 1996, ApJ, 471, 115
 Benson, A.J., Kamionkowski, M., Hassani, S.H. 2005, MNRAS, 357, 847
 Benson, A.J., Nusser, A., Sugiyama, N., Lacey, C.G., 2001, MNRAS, 320, 153
 Benson, A.J., Nusser, A., Sugiyama, N., Lacey, C.G., 2006, MNRAS, 369, 1055
 Bond, J.R., Cole S., Efstathiou G., Kaiser N. 1991, ApJ, 379, 440
 Bower, R.G. 1991, MNRAS, 248, 332
 Bullock, J.S. et al. 2001, MNRAS, 321, 559
 Busha, M.T., Evrard, A.E., Adams, F.C., Wechsler, R.H., 2005, MNRAS, 363, L11
 Carlberg, R.G., 1990, ApJ, 350, 505
 Casas-Miranda, R., Mo, H.J., Sheth, R.K., Börner, G., 2002, MNRAS 333, 730
 Cavaliere, A., Vittorini, V., 2000, ApJ, 543, 599
 Ciardi, B., Stoehr, F., White, S.D.M., 2003, MNRAS, 343, 1101
 Cohn, J.D., Bagla, J.S., White, M., 2001, MNRAS, 325, 1053
 Cohn, J.D., Chang, T.-C., 2007, MNRAS, 374, 72
 Cohn, J.D. White, M. 2005, APh, 24, 316
 Cole, S., Kaiser, N., 1989, MNRAS, 237, 1127
 Cole, S., Lacey, C., 1996, MNRAS, 281, 716
 Cooray, A., Barton, E., eds., 2005, "First Light and Reionization: Theoretical Study and Experimental Detection of the First Luminous Sources", New AR 50
 Conselice, C.J., 2006, ApJ 638, 686
 Davis, M., Efstathiou, G., Frenk, C.S., White, S.D.M. 1985, ApJ, 292, 371
 Efstathiou, G., et al. 1988, MNRAS, 235, 715
 Evrard et al. 2007, preprint [astro-ph/0702241]
 Fan, X., Carilli, C.L., Keating, B., 2006, ARA&A 44, 415
 Furlanetto, S.R., Hernquist, L., Zaldarriaga, 2004a, MNRAS, 354, 695
 Furlanetto, S.R., McQuinn, M., Hernquist, L., 2006, MNRAS 365, 15

- Furlanetto, S.R., Oh, S.P., 2005, MNRAS 363, 103
- Furlanetto, S.R., Oh, S.-P., Briggs, F., 2006, Phys. Rep. 433, 181.
- Furlanetto, S.R., Zaldarriaga, M., Hernquist, L., 2004b, ApJ 613, 1
- Furlanetto, S.R., Zaldarriaga, M., Hernquist, L., 2004c, ApJ 613, 16
- Furlanetto, S.R., Zaldarriaga, M., Hernquist, L., 2006, MNRAS, 365, 1012
- Gnedin, N.Y. 2000, ApJ, 535, 530
- Gottlöber, S., et al. 2002, A&A, 387, 778
- Heitmann, K., Lukic, Z., Habib, S., Ricker, P.M., 2006, ApJL 642, 85
- Heitmann, K., et al., 2007, to appear in Computational science and discovery, arxiv/0706.1270.
- Hu, W., Kravtsov, A.V., 2003, ApJ, 584, 702
- Iliev, I.T., et al, 2005, MNRAS 361, 405
- Iliev, I. T., Mellema, G., Pen, U.-L., Merz, H., Shapiro, P. R., Alvarez, M.A., 2006a, MNRAS, 369, 1625
- Iliev, I.T., et al, 2006b, MNRAS, 371, 1057
- Iliev, I.T., Melleman, G., Pen, U.-Li., Bond, J.R., Shapiro, P.R., 2007, preprint [astro-ph/0702099]
- Jang-Condell, H., Hernquist, L., 2001, ApJ, 548, 68
- Jenkins, A., Frenk, C. S., White, S. D. M., Colberg, J. M., Cole, S., Evrard, A. E., Couchman, H. M. P., Yoshida, N., 2001, MNRAS, 321, 372
- Jing, Y.P., 1998, ApJ, 503, L9
- Kaiser, N. 1984, ApJ, 284, L9
- Kauffmann, G., Haehnelt, M. 2000, MNRAS, 311, 576
- Kauffmann, G., et al., 2003, MNRAS 341, 54.
- Kitayama, T., Suto, Y. 1996a, MNRAS, 280, 638
- Knebe, A., Muller, V., 1999, A&A, 341, 1
- Kohler, K, Gnedin, N.Y., Hamilton, A.J.S, 2005, preprint [astro-ph/0511627]
- Lacey, C.G., Cole S. 1993, MNRAS, 262, 627
- Lacey, C.G. Cole, S. 1994, MNRAS, 271, 676
- Li, Y., Mo, H.J., van den Bosch, F.C., Lin, W. P., 2006, MNRAS, in press [astro-ph/0510372]
- Lukic, Z, Heitmann, K, Habib, S, Bashinsky, S., Ricker, P.M., 2007, preprint [astro-ph/0702360]
- Madau, P., Rees, M.J., Volonteri, M., Haardt, F., Oh, S.P., 2004, ApJ 604, 484
- Maio, U., Dolag, K., Meneghetti, M., Moscardini, L., Yoshida, N., Baccigalupi, C., Bartelmann, M., Perrotta, F., 2006, MNRAS 373, 869
- McQuinn, M., Lidz, A., Zahn, O., Dutta, S., Hernquist, L., Zaldarriaga, M., 2007, MNRAS, 377, 1043 [astro-ph/0610094]
- Mellema, G., Iliev, I.T., Pen, U.-L., Shapiro, P.R., 2006, MNRAS 372, 679
- Mesinger, A., Furlanetto, S., 2007, preprint [arXiv:0704.0946]
- Mihos, J., Hernquist, L. 1994, ApJ, 425, 13
- Mihos, J., Hernquist, L. 1996, ApJ, 464, 641
- Miller, L., Percival, W.J., Croom, S.M., Babic, A. 2006, A & A to appear, preprint [astro-ph/0608202]
- Mo, H.-J., White, S.D.M., 1996, MNRAS, 282, 347
- Navarro, J.F., Frenk, C.S., White, S.D.M., 1997, ApJ, 490, 493
- Neistein, E., van den Bosch, F. C., Dekel, A., 2006, MNRAS 372, 933
- Peacock J., 1998, "Cosmological Physics", Cambridge University Press (Cambridge, UK)
- Percival, W., 2001, MNRAS 327, 1313
- Pervial, W.J., Miller, L., Peacock, J.A., 2000, MNRAS, 318, 273
- Percival, W.J., Scott, D., Peacock, J.A., Dunlop, J.S. 2003, MNRAS, 338L, 31
- Press, W., Schechter, P., 1974, ApJ, 187, 425
- Reed, D., et al., 2003, MNRAS 346, 565
- Reed, D., et al., 2005, MNRAS 363, 393
- Reed, D. S., Bower, R., Frenk, C. S., Jenkins, A., Theuns, T., 2007, MNRAS, 374, 2
- Scannapieco, E., Thacker, R.J. 2003, ApJ, 590, L69
- Seljak, U., Warren, M.S. 2004, MNRAS, 355, 129
- Shaw, L.D., Weller, J., Ostriker, J.P., Bode, P., 2006, ApJ, 646, 815
- Shen Y., et al., 2007, preprint [astro-ph/0702214]
- Sheth, R.K., Lemson, G., 1999, MNRAS, 304, 767
- Sheth, R.K., Mo, H.-J., Tormen, G., 2001, MNRAS, 323, 1
- Sheth, R.K., Pitman, J., 1997, MNRAS, 289, 66
- Sheth, R.K., Tormen, G. 1999, MNRAS, 308, 119
- Smoot, G.F., et al., 1992, ApJ, 396, L1
- Sokasian, A., Abel, T., Hernquist, L., Springel, V., 2003, MNRAS, 344, 607
- Sokasian, A., Yoshida, N., Abel, T., Hernquist, L., Springel, V., 2004, MNRAS, 350, 47
- Somerville, R.S., Lemson, G., Kolatt, T., Dekel, A., 2000, MNRAS 316, 479
- Springel, V., et al., 2005, Nature, 435, 629
- Tinker, J.L., Weinberg, D.H., Zheng, Z., Zehavi, I., 2005, ApJ, 631, 41
- Trac, H., Cen, R., 2006, preprint [astro-ph/0612406]
- Tormen, G., 1998, MNRAS 297, 648
- Wang H.Y., Mo H.J., Jing Y.P., 2006, preprint [astro-ph/0608690]
- Warren, M.S., Abazajian, K., Holz, D.E., Teodoro, L., 2005, preprint [astro-ph/0506395]
- Wechsler, R. H. et al. 2002, ApJ, 568, 52
- Wetzel, A.R., Cohn, J.D., White, M., Holz, D.E., Warren, M.S., 2007, ApJ 656, 139
- White, S.D.M. 1993, Les Houches Lectures.
- White, M. 2001, A&A, 367, 27
- White, M. 2002, ApJS, 579, 16
- White, M., Martini, P., Cohn, J.D., 2008, submitted to MNRAS [arxiv/0711.4109]
- Wyithe, S.B., Loeb, A., 2003, ApJ, 586, 693
- Yoshida, N., Bromm, V., Hernquist, L., 2004, ApJ 605, 579
- Zahn, O., et al., 2005, ApJ, 630, 657
- Zahn, O., Lidz, A., McQuinn, M., Dutta, S., Hernquist, L., Zaldarriaga, M., Furlanetto, S.R., 2007, ApJ, 654, 12
- Zaldarriaga, M., Furlanetto, S., Hernquist, L., 2005, ApJ 608, 622
- Zentner, A.R., 2006, preprint [astro-ph/0611454]